Received: 31 July 2024 | Revised: 4 September 2024 | Accepted: 12 September 2024

DOI: 10.1002/pen.26982

RESEARCH ARTICLE

POLYMER ENGINEERING AND SCIENCE WILEY

Effect of β nucleating agent and rotational shear on morphology and mechanical properties of polypropylene pipes

Aerman Abudurezhake[1] | Minghao Yang[1] | Jiawei Gong[2] | Ganji Zhong[1] | Zhongming Li[1] | Qiang Fu[1] | Xueqin Gao[1]

[1]College of Polymer Science and Engineering, Sichuan University, Chengdu, China

[2]Department of Mechanical Engineering, Pennsylvania State University, Erie, Pennsylvania, USA

Correspondence
Xueqin Gao, College of Polymer Science and Engineering, Sichuan University, Chengdu 610065, China.
Email: gaoxueqin@scu.edu.cn

Funding information
National Natural Science Foundation of China, Grant/Award Numbers: 52373045, 12375332, 52033005, 21627804

Abstract

Herein, we report a new method of introducing circumferential shear to polypropylene (PP) pipes via a self-designed rotational shear system (RSS) with the addition of a β-nucleating agent (TMB-5). The prepared PP pipes exhibited remarkable enhancement in toughening and tensile strength over conventional PP pipes incorporating 0.025 wt% of the nucleating agent into the sheared sample increased the elongation at break to 243.30%. At 0.05 wt% nucleating agent content, an optimal tensile strength of 40.98 MPa was attained compared to 33.62 MPa for unsheared PP, and the elongation at break also reached 108.09%. In creep tests, the PP pipes prepared with nucleating agents and shear rotation exhibited a minimum displacement of 2.1 mm and the lowest creep rate of 3.23×10^{-5} mm/s. In addition, the samples also showed a high resistance to crack growth compared to conventional PP pipes with a crack initiation time of 24 h and a crack growth rate of 0.08 mm/s.

Highlights

- Reinforced and toughened PP pipes were prepared using a rotational shear system.
- The shish-kebab structure and β-crystals exhibited a synergistic effect.
- Both short-term and long-term mechanical properties were studied.

KEYWORDS

elongation at break, PP pipes, rotational shear, tensile strength

1 | INTRODUCTION

Polypropylene (PP) has been widely used for drainage pipelines due to its low cost, chemical resistance, and excellent processability.[1] Traditional pipe extrusion processes tend to align PP molecular chains along the extrusion direction, resulting in superior axial strength. However, under operating conditions, pipelines are subjected to circumferential stress that is twice the axial stress.[2] Additionally, α-spherulites formed in PP pipes lead to relatively low toughness. The poor circumferential strength and low toughness of PP pipes under high sustained stress limit their lifespan. Thus, the improvement of the above performance-limiting factors has the potential to increase the service life of pipes, reduce maintenance costs, and achieve more environmentally friendly applications.

A promising technique to simultaneously improve the circumferential strength and toughness is through

rotational extrusion with the addition of β-nucleating agents. Conventional PP contains predominantly α-crystals that are densely packed with fewer intercrystalline contacts. The well-defined interfaces are prone to crack initiation under rapid external loads.[3] In contrast, the β-crystal structure is less densely packed and offers mobility of molecular chains. Micropores formed in such microstructures allow plastic deformation and absorb impact energy, resulting in better toughness.[4] Nevertheless, an excessive amount of β-crystals can significantly reduce the strength of the pipes, and therefore, must be avoided. Several studies[5,6] have indicated that high shear forces can suppress the generation of β-crystals in PP. Moreover, under the external force field, the polymer's unique long-chain structure will be arranged along the direction of the flow field, forming an orientated or shish-kebab structure, which has been recognized to greatly improve the mechanical properties of the material.[7,8] These insights lead to the approach of combining extrusion with the addition of β-nucleating agents under a rotational field to enhance molecular chain orientation and avoid excessive generation of β-crystals, which is suitable for preparing high-strength and high-toughness PP pipes.

Besides, PP pipes are often used in low-temperature, low-pressure environments for an extended period. Cracks initiated at stress concentration points develop and propagate over time, leading to brittle failure. This is known as slow crack growth, the primary failure mode of plastic pipes. Another concern for the long-term use of PP pipes is a creep, which stems from the viscoelasticity of polymers. The creep-caused deformation in PP pipes can compromise the structural integrity and the sealing capacity of pipe joints after long-term stress. The single study of short-term mechanical properties cannot provide sufficient data support for the long-term service of the pipes, so the study of long-term mechanical properties becomes particularly important, which well shows the structural changes of the material under long-term stress. Research[9] indicates that highly oriented fibers can withstand greater external stresses, significantly increasing creep resistance. Both crystalline regions and amorphous regions in PP play crucial roles in resisting creep.[10] Our previous work successfully increased the yield strength of the β-nucleated isotactic PP by generating β crystals and inducing crystal orientation by applying a vibration shear field using a homemade Vibration-assisted Extrusion Apparatus.[11] However, this increase in strength sacrifices the elongation at break. Furthermore, Wang et al.[12,13] have prepared high-performance HDPE and PP pipes by adjusting the rotational speed of an extruder head with a mandrel and die that can rotate in the same direction to improve the molecular chain orientation. We discovered that PP pipes prepared under rotational shear fields have significant differences in their microstructures compared to conventional pipes.[14,15] Therefore, the potential microstructural and performance changes of β-nucleated isotactic PP under rotational shear fields have aroused our widespread interest.

As a widely used product, it is particularly significant to improve the performance of PP pipes in a targeted manner, taking into account the operating conditions and the performance shortcomings of the material itself. In this study, we adopted a rotational shear system (RSS) to exert circumferential shear on β-nucleated PP pipes via an externally applied rotational field. By comparing with conventional PP pipes, the synergistic effect of crystal structure improvement and molecular chain orientation on the long- and short-term mechanical properties of pipes under rotational shear was systematically studied, and the mechanism was elucidated. We aim to optimize the performance of PP pipes, providing guidance for developing high-performance polymer piping materials and novel processing methods.

2 | EXPERIMENT

2.1 | Material

Isotactic PP (iPP) was provided by Lanzhou Petrochemical Co., Ltd. The grade is T30, with a density of 0.91 g/cm^3 and a melt index of 2.60 g/10 min. The β-nucleating agent was TMB-5, an amide-type nucleating agent provided by the Shanxi Provincial Institute of Chemical Industry Co., Ltd. During the processing, TMB-5 dissolves in the resin melt and forms rod-shaped crystals with a relatively large aspect ratio, thereby facilitating nucleation and subsequent crystallization.

2.2 | Apparatus and sample preparation

The process of blending iPP with TMB-5 was conducted using a twin-screw extruder manufactured by China Bluestar Chengrand Co., Ltd. The extruder has a screw diameter of 25 mm, a length-to-diameter ratio of 33. There are seven temperature control zones along the barrel with a heating capacity of 10 kW. During blending, the temperatures of the extruder zones were adjusted progressively from the hopper to the die, starting at 150°C and increasing to 180, 185, and 190°C (maintained across three zones), and finally 200°C at the die. The twin-screw extruder operated at a rotational speed of 132 rpm while the pelletizer was set to 120 rpm.

To ensure uniform dispersion of TMB-5 in iPP, a masterbatch was prepared with 2 wt% TMB-5, which was then blended with pure iPP to achieve the desired ratio. A

previous study[16] showed that PP structures in the presence of TMB-5 vary with the nucleating agent content. Below the subcritical content, quasi-spherulites are primarily formed, while above the subcritical content but below the supercritical content, microcrystals are generated. Above the supercritical content, crystallization occurs on the surface of the nucleating agent crystals. Our experiment investigated the structural variations across a range of nucleating agent contents, specifically 0.025, 0.05, 0.1, and 0.2 wt%, following a logarithmic distribution. The pure iPP was used as the control sample and designated as 0 wt%.

After blending, the mixture was dried in a constant temperature blast dryer set at 80°C for 6 h. A self-made RSS, as illustrated in Figure 1, was utilized to extrude PP pipes with an outer diameter of 63 mm and a thickness of 3 mm. This apparatus ensures consistent circumferential shear stress throughout the plasticization and extrusion process. For sample preparation, the extruder temperatures were set at 145, 205, 220, and 210°C from hopper to die, respectively. Once the temperature of the mold core reached 150°C, the extruder was activated to transfer the plasticized polymer melt into the mold cavity, and the cooling device was activated. Upon filling the mold, the screw began to rotate at a speed of 6 rpm. The rotation of the mandrel stopped when the cavity temperature dropped to 132°C, and the shearing duration was 90 s. The cooling system was deactivated when the temperature reached 110°C (Figure 1).

2.3 | Characterizations

2.3.1 | X-ray diffraction

The experiment on synchrotron two-dimensional wide-angle X-ray diffraction (2D-WAXD) was carried out at the BL16B1 beamline of the Shanghai Synchrotron Radiation Facility (SSRF) located in Shanghai, China. The light source had a wavelength of 0.124 nm, and the samples were exposed for a duration of 5 s. The beam was rectangle-shaped with a dimension of 0.3 × 0.5 mm. The sample-to-detector distance was 140 and 1900 mm for wide-angle X-ray diffraction (WAXD) and small-angle X-ray scattering (SAXS), respectively.

Linear WAXD profiles were obtained from the circular integration of intensities from 2D-WAXD images. The intensity was plotted as a function of the scattering vector, q, where $q = 4\pi \sin\theta/k$, with k being the wavelength of the incident beam and 2θ being the scattering angle. Subsequently, through deconvolution of the diffraction peaks in the linear WAXD profiles, the relative amount of β-phase (K_β) was calculated by the widely accepted formula proposed by Turner-Jones and Cobbold[17]

$$k_\beta = \frac{A_\beta(300)}{A_\beta(300) + A_\alpha(110) + A_\alpha(040) + A_\alpha(130)} \quad (1)$$

where A_α (110), A_α (040), and A_α (130) are the intensities for α-form peaks at the (110), (040), and (130) planes, respectively, while A_β (300) is the intensity of β-form peak (300), as observed in the 1D-WAXD pattern.

The orientation parameter of crystals was evaluated using Herman's method, which was defined as follows:

$$f = \frac{3(\cos^2\varphi) - 1}{2} \quad (2)$$

where $\cos^2\varphi$ is an orientation factor defined as follows:

$$(\cos^2\varphi) = \frac{\int_0^{\frac{\pi}{2}} I(\varphi)\sin\varphi\cos^2\varphi d\varphi}{\int_0^{\frac{\pi}{2}} I(\varphi)\sin\varphi d\varphi} \quad (3)$$

where φ is the angle between the normal of a given (hkl) crystal plane and the direction of shear flow, and $I(\varphi)$

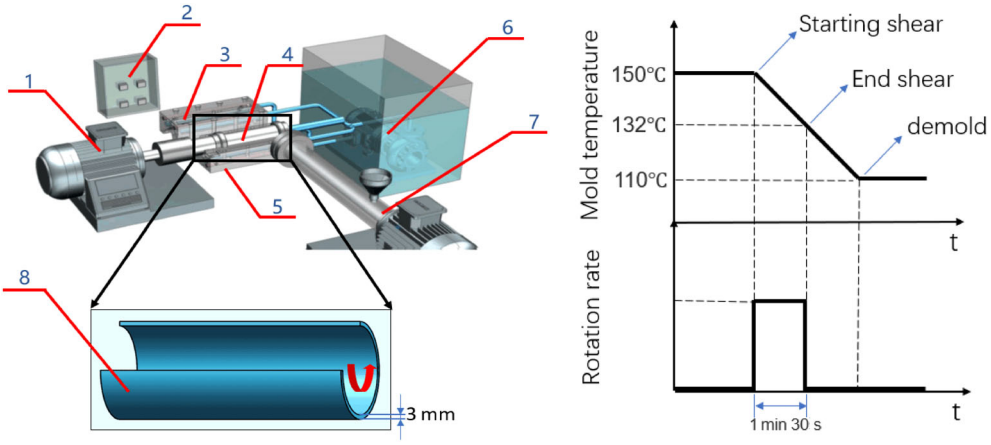

FIGURE 1 Schematic diagram of the rotational shear system and process flowchart: 1, Motor; 2, Heating control system; 3, Upper mold; 4, Mandrel; 5, Lower mold; 6, Cooling system; 7, Plasticizing system; 8, Pipe.

represents the diffraction intensity. The (040) diffraction rings in the two-dimensional patterns were chosen for calculating the degree of orientation in this study.[18]

From 2D-SAXS images, a small angle curve can be derived, and then the long-period l_{ac} can be obtained according to the Bragg formula:

$$l_{ac} = \frac{2\pi}{q_{max}} \tag{4}$$

Grzzuti[19] proposed a micro-rheological theory to describe the crystallization induced by external force based on the Doi–Edwards (*De*) theory, considering the competition between molecular chain stretching and relaxation in the formation of spherulites. This competition can be quantitatively described using the *De* value:

$$De = \gamma \cdot \tau_d \tag{5}$$

where γ is the shear rate and τ_d is the molecular chain end relaxation time. Only when $De < 1$, the effect of the external force field on the molecular chain is dominant and the elongational deformation can be retained, eventually leading to the formation of spherulites. Numerous experiments[19–21] have confirmed that the larger the *De* value, the easier it is to form spherulites.

2.4 | Differential scanning calorimetry

The crystallinity of the samples was assessed through differential scanning calorimetry (DSC) using a TA Instruments Q200 model. The testing conditions involved heating the sample from room temperature to 200°C at a rate of 10°C/min.

The degree of crystallinity (X_c) was calculated using the following equation:

$$X_c = \frac{\Delta H_m}{\Delta H_m^0} \tag{6}$$

where ΔH_m is the measured enthalpy of fusion of the test sample and ΔH_m^0 is the standard enthalpy of fusion for fully crystalline PP, with a value of 207 J/g.

2.5 | Scanning electronic microscopy

Scanning electronic microscopy (SEM) observations were conducted using a JEOL field emission SEM (model JSM-7500F, Japan). Samples were cut from the pipes along the axial direction, chemically etched with a mixed acid solution after polishing, and finally sputter-coated with gold.

2.6 | Mechanical properties

Circular rings approximately 8 mm in length were cut along the axial direction of the pipe for radial tensile testing at room temperature. Due to the inability of the circular ring samples to be firmly gripped by the conventional dumbbell-shaped specimen grips of the tensile machine, we customed fixtures for holding the circular rings, as shown in Figure 2. Note that during the tensile process, the circular ring is subjected to tension at both ends until it breaks, so the force area is calculated by doubling the cross-sectional area of the ring. The tensile tests were performed on Shimadzu AGS-J desktop universal material testing machine with a set extension rate of 10 mm/min. Five tests were conducted per specimen, and the average values were reported.

2.7 | Creep testing

The creep behavior of the pipes was investigated using a custom-made creep testing apparatus, as shown in Figure 3. This apparatus consists of a temperature control unit, a displacement acquisition system, and a sample clamp. Similar to the tensile test samples, the pipes were cut into 8 mm thick circular rings. The specimens, clamped on the fixture, were pre-loaded and placed in the constant temperature chamber at 80°C. Subsequently, the displacement data was captured every 5 s and logged onto a computer system. The pre-defined load was set at 10 MPa, comprising the combined weight of the connecting rod, balance, and additional weights. The tests continued until the specimen was pulled apart, lasting approximately 28 h.

For data processing, we utilize the following equations:

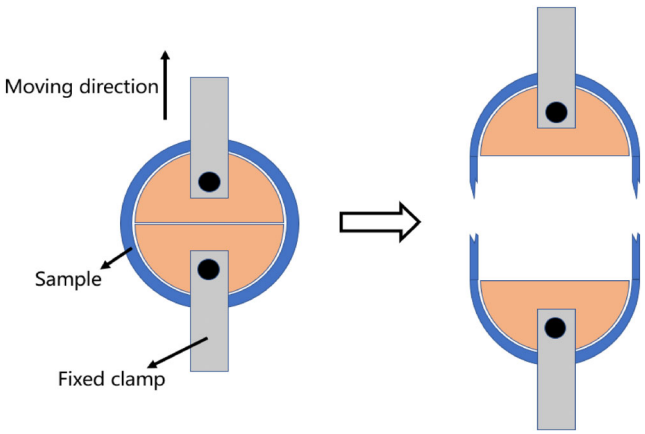

FIGURE 2 Schematic diagram of tensile test setup.

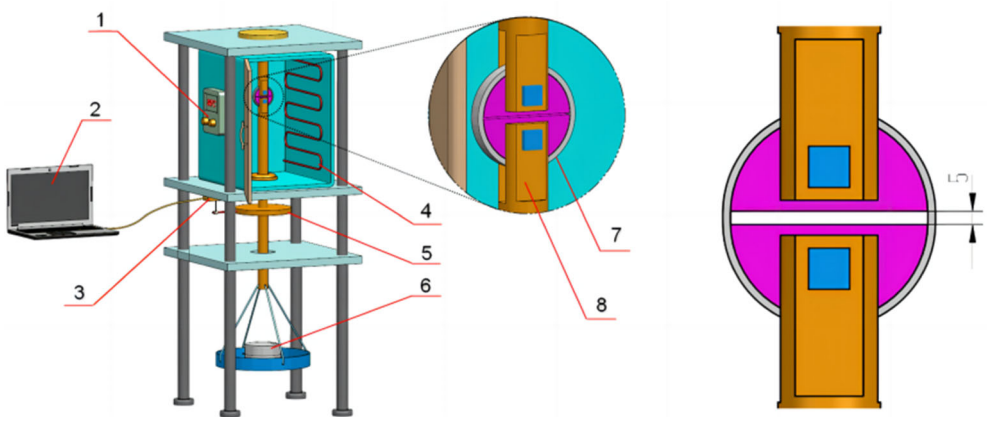

FIGURE 3 Creep testing apparatus schematic diagram: 1, Temperature control unit; 2, Displacement acquisition system (computer); 3, Displacement sensor; 4, Heating wire; 5, Spacing table; 6, Weights; 7, Pipe; 8, Fixture.

1. Strain is defined as the ratio between elongation (Δl) over the original gauge length (L), $\varepsilon = \frac{\Delta l}{L}$. To ensure a smooth fit of samples into the circular fixture, the diameter of the fixture was designed to be slightly smaller than the diameter of the pipe. This gives some clearance between the circular ring and the fixture. When there is no load applied, the two halves of the fixture can be displaced by 5 mm. Thus, in this experiment, the gauge length of the specimen is taken as $L = 5$ mm.
2. Compliance is defined as the change in strain as a function of time under instantaneous application of a constant stress, $J(t) = \frac{\varepsilon(t)}{\sigma_0}$, where $\sigma_0 = 10$ MPa.
3. Creep rate: The creep rate is defined as the elongation per unit time under a certain stress. The total creep time of the experiment was set to 30,000 s with the fixed stress as 10 MPa.

2.8 | Slow crack growth testing

The slow crack growth experiment on PP pipes was conducted in compliance with GB/T 19279-2003 standards. A 70-mm length pipe ring specimen was cut from the pipe, and a brass cone slightly larger than the inner diameter of the pipe was inserted to maintain a predetermined strain. Subsequently, an initial notch of 10 mm was cut at one end of the pipe ring specimen, as depicted in. For the sample pretreatment, the specimen was immersed in a solution containing a surfactant at a concentration of 10% atperature of 80 ± 1°C. The complete apparatus setup is illustrated in Figure 4.

3 | RESULTS AND DISCUSSION

3.1 | WAXD analysis

Figure 5(A) presents the WAXD images collected from PP specimens with and without rotation. The diffraction rings from inner to outer correspond to different crystal planes of PP, namely: α (110), β (300), α (040), α (111), α (130), α (−131/311), α (060), and α (220). Diffraction rings were clearly observed in all specimens. Specimens subjected to rotation exhibit arc-like diffraction patterns for all crystal planes, indicating the presence of aligned molecular chains, whereas the static specimens (0 rpm) show isotropic diffraction patterns for all crystal planes. There were no β crystals formed in static and rotating conditions when pure PP (0% TMB-5) was used, as confirmed by the absence of the β (300). With the addition of β-NA, β (300) planes appear in all static specimens, with this plane showing the highest brightness, indicating abundant β crystals. This is related to the efficient nucleating agent TMB-5, which induces significant β crystal formation with only a trace amount. However, once a rotating field is applied, the intensity of β (300) planes significantly decreases.

To further obtain the crystallinity content, one-dimensional wide-angle curves were obtained by integrating the corresponding WAXD patterns, as shown in Figure 5(b–e). The crystallinity content of the middle layer in static specimens was obtained through this curve, as listed in Table 1. The incorporation of β-NA into static specimens drastically increased the crystallinity content from 0% to 50.41%. With an increase in β-NA content, the crystallinity content showed an initial increase followed by a decrease trend, reaching a maximum value of 78.25% when β-NA was at 0.05 wt%. This may be related to the solubility of β-NA in the PP matrix. At lower contents, β-NA can dissolve completely in PP, leading to good dispersion in PP and thus inducing the formation of crystal structures. However, at higher contents, β-NA cannot be well mixed with the PP matrix, leading to aggregation. This phenomenon can be clearly observed in the hot-stage polarized images, as shown in Figure 5(F–H). Pure PP specimens uniformly exhibit a relatively homogeneous morphology. For a content of 0.05 wt% β-NA, it dissolves completely in PP, while for

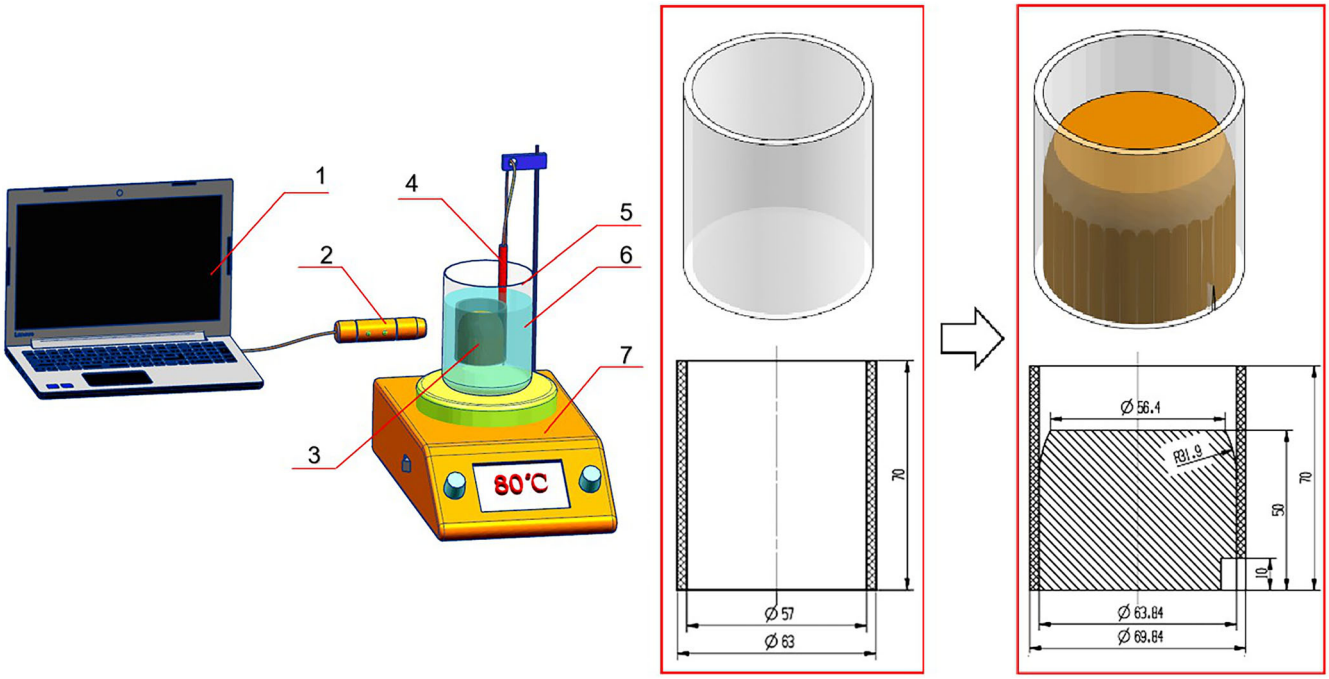

FIGURE 4 Slow crack growth testing apparatus: 1, Image collection system (computer); 2, Compound digital microscope; 3, Sample; 4, Thermocouple; 5, Large beaker; 6, Solution; 7, Magnetic stirrer.

higher contents like 0.2 wt%, the image shows the obvious precipitation and aggregation of β-NA. Therefore, in this experiment, contents exceeding 0.05 wt% lead to excessive aggregation, which is the main reason for the decrease in crystallinity content.

For the specimens subjected to rotational shear with β nucleating agents added, peaks of β (300) crystal planes are also present in the inner, middle, and outer layers, but they are not particularly pronounced. Previous studies[5,6,22,23] have also reported that high shear rates inhibit the formation of β crystals in PP containing β nucleating agents. This could be due to the fact that during the crystal growth process, shear further induces the formation of more α crystal nuclei, and their growth rate exceeds that of β crystals, rapidly occupying limited space, resulting in a decrease in β crystallinity content. In this study, the rotational speed of 6 rpm was relatively high, thereby inhibiting crystal formation.

Two crystal planes, namely α (040) and β (330) were selected for calculating the degree of orientation for α-crystal and β-crystal, respectively. It should be noted that for rotating specimens without the addition of β-NA, β-crystals are completely absent. The azimuthal angle curves corresponding to each crystal plane were presented in Figure 6(A–C, E–G) based on the empirical formula: $\Pi = \frac{180^\circ - H}{180^\circ} \cdot 100\%$, where H is the half-width at half-maximum of the intensity distribution curve of the Debye rings on the equator. The obtained orientation degrees are shown in Figure 6(D, H). The results show that both the orientation degrees of α-crystal and β-crystal are lowest in the inner layer. It contradicts the simulation results of the shear rate distribution, in which the shear rate in the inner layer appears to be the highest, suggesting that the orientation degree should be higher in the inner layer. The discrepancy may result from the limitations of the apparatus, specifically the use of thermal oil for temperature control around the core rod rather than heating rods for the external mold temperature control, causing the temperature not to reach the desired level. Therefore, during the gradual cooling and shearing process, the inner layer close to the core rod may solidify prematurely, experiencing a much shorter shearing time, thus resulting in a minimal orientation degree. The shear rate in the middle layer is higher than that in the outer layer; however, rapid solidification in the middle layer shortens the shearing duration compared to the outer layer, leading to similar orientation degrees of the middle layer and the outer layer.

Furthermore, with the increase in β-NA content, the orientation degree shows a trend of initial increasing and then decreasing, reaching a maximum value at 0.05 wt% content. Based on rheological data (Figure S1), we obtained the relaxation time of samples with different β-NA contents, as shown in Figure 7(A). With the increase in β-NA content, the relaxation time of the PP matrix continuously decreases, from 0.47 s^{-1} for pure PP to 0.14 s^{-1}. Figure 7(B) presents the Cole-Cole plots for the complex viscosity (η'') versus intrinsic viscosity (η') curves for different β-NA contents. The magnitude of their arc radius can also reflect the rate of molecular

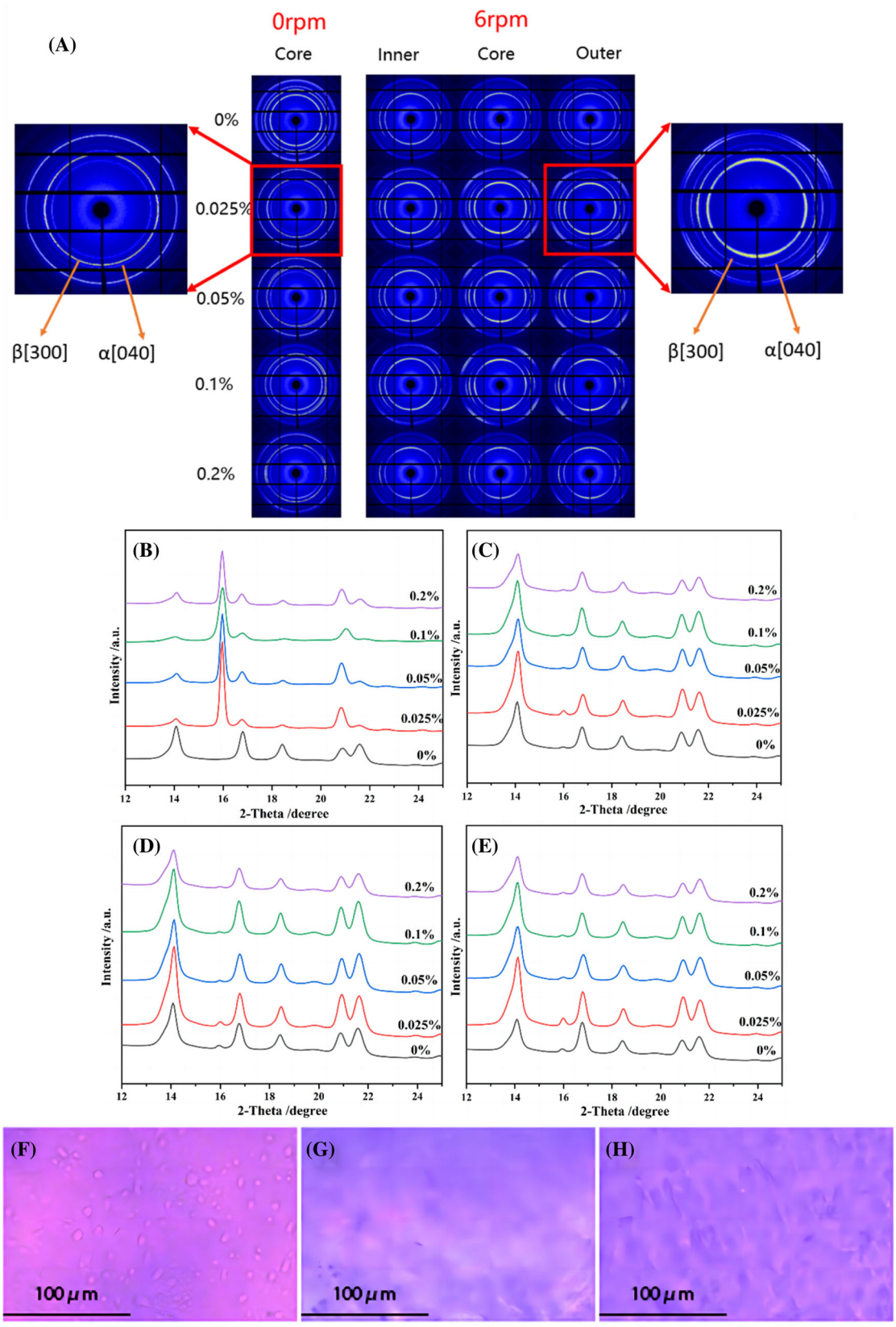

FIGURE 5 The two-dimensional wide-angle X-ray diffraction (WAXD) analysis and thermal stage polarized images: (A) WAXD images of PP pipes with different nucleating agent contents; (B) integrated curves of 0 rpm—middle layer; (C) integrated curves of 6 rpm—inner layer; (D) integrated curves of 6 rpm—middle layer; (E) integrated curves of 6 rpm—outer layer; (F) thermal stage polarized images of 0 wt%; (G) thermal stage polarized images of 0.05 wt%; and (H) thermal stage polarized images of 0.2 wt%.

β nucleating agent content	The relative content of β-crystals			
	0 rpm		6 rpm	
	Core	Inner	Core	Outer
0 wt%	0%	0%	0%	0%
0.025 wt%	50.41%	1.60%	1.12%	2.26%
0.05 wt%	78.25%	0.35%	0.30%	0.85%
0.1 wt%	65.55%	0.33%	0.30%	0.53%
0.2 wt%	53.89%	0.70%	0.63%	0.93%

TABLE 1 The crystalline phase content of PP pipes with different β nucleating agent contents.

chain relaxation.[7,24] The arc radius is largest for pure PP, while it is smallest for PP with 0.02 wt% β-NA content, indicating that the former has the longest chain relaxation time, and the latter has the shortest. With the increase in β-NA content, the arc radius of PP decreases, implying that molecular chain relaxation is facilitated, which is consistent with the calculated relaxation rate. Therefore, for the middle layer and the outer layer, with the increase in β-NA content, on the one hand, the shear rate increases, leading to higher molecular chain orientation; on the other hand, the relaxation time decreases, making it less likely for the molecular chain orientation to be maintained. These two competing factors result in the highest orientation degree at 0.05 wt% content.

3.2 | SAXS analysis

The results of SAXS testing on static and rotating shear specimens are shown in Figure 8(A). For static specimens, pure PP exhibits uniform scattering rings, while PP specimens with added β-NA show uneven diffraction signals, which may be largely related to the morphology of β-NA.[25,26] Aggregation of β-NA in the PP matrix leads to anisotropic behavior. As for the rotating shear specimens, they all exhibit certain scattering intensity in the meridian direction, indicating the generation of lamellar crystals perpendicular to the shear direction, known as the "kebab" structure, and the intensity increases significantly with the addition of β-NA. In the equatorial direction, needle-like diffraction signals indicate the formation of "shish" structures along the flow direction.

Based on the shear rate data simulated using Polyflow (Supplementary Flow Simulation) and the relaxation time data obtained from rheology (Figure 7), we calculated the *De* value for the inner layer, as shown in Table 2. It can be observed that only when the β-NA content is 0.2 wt%, $D_e < 1$, indicating that there is no formation of spherulites. Therefore, only when the content is 0.2 wt%, there is no needle-like diffraction signal in the equatorial direction. It is worth mentioning that our previous work using a Vibration-Assisted Extrusion Apparatus did not generate the "shish-kebab" structure,[11] which provides a molecular basis for the performance differences caused by two different shear fields in subsequent experiments.

To analyze grain size, we derived Lorenz-corrected one-dimensional small-angle diagrams from the two-dimensional small-angle diagrams and then calculated the long period of the sample. For static samples (0 rpm) as shown in Figure 8(B,D), the long period in the equatorial and meridian direction significantly increases from 3.01 and 3.11 nm to 3.88 and 3.81 nm, respectively, with the increase in β-NA content for 0% to 0.05%. The initial increase, followed by a decrease, was mainly due to the different structures of α and β crystals. Monoclinic α crystals have lattice parameters: a = 0.665 nm, b = 2.096 nm, and c = 0.650 nm, whereas trigonal β crystals have lattice parameters: a = 1.102 nm, b = 1.102 nm, and c = 0.649 nm.[27,28] Although compared to β crystals, α crystals have larger lattice parameters, the β crystals have larger nucleus density, smaller grain size, and no obvious boundary between the interfaces. Therefore, the long period will be relatively long and should align with the trend of crystal content changes. Thus, it is evident that with the addition of β-NA, the increase in the long period of static samples benefits from the increase in crystal content. In addition, at a high nucleating agent content of 0.2 wt%, the nucleation density further increases, and in a limited crystal growth space, a smaller crystal is formed, resulting in little change in the long period or even a decrease in the meridian direction. As for rotating samples (6 rpm), as shown in Figure 8(C,E), the β crystal content is only about 2%, and the effect on the long period is insignificant. However, it also showed the same trend as the static sample, that is, with the increase of nucleating agent content, the long period increased first and then decreased. This is mainly because the average long period of oriented crystals is greater than that of non-oriented crystals,[29] so the long period should be consistent with the degree of

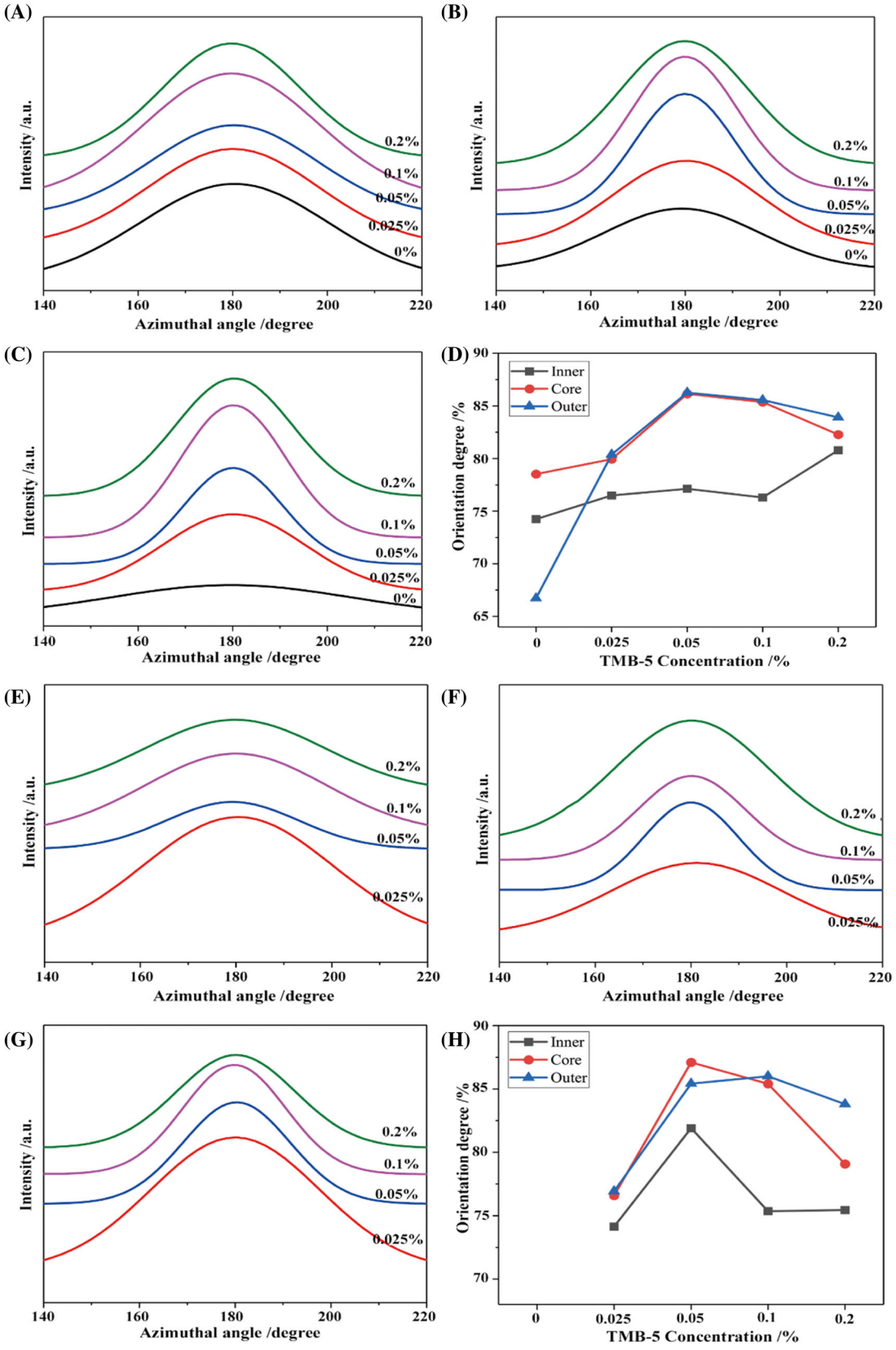

FIGURE 6 The azimuthal angle and orientation degree of the α (040) and β (300) crystal plane in rotating PP pipes with different β nucleating agent contents: (A) azimuthal angle of α (040) inner layer; (B) azimuthal angle of α (040) middle layer; (C) azimuthal angle of α (040) outer layer; (D) orientation degree of α (040); (E) azimuthal angle of β (300) inner layer; (F) azimuthal angle of β (300) middle layer; (G) azimuthal angle of β (300) outer layer; and (H) orientation degree of β (300).

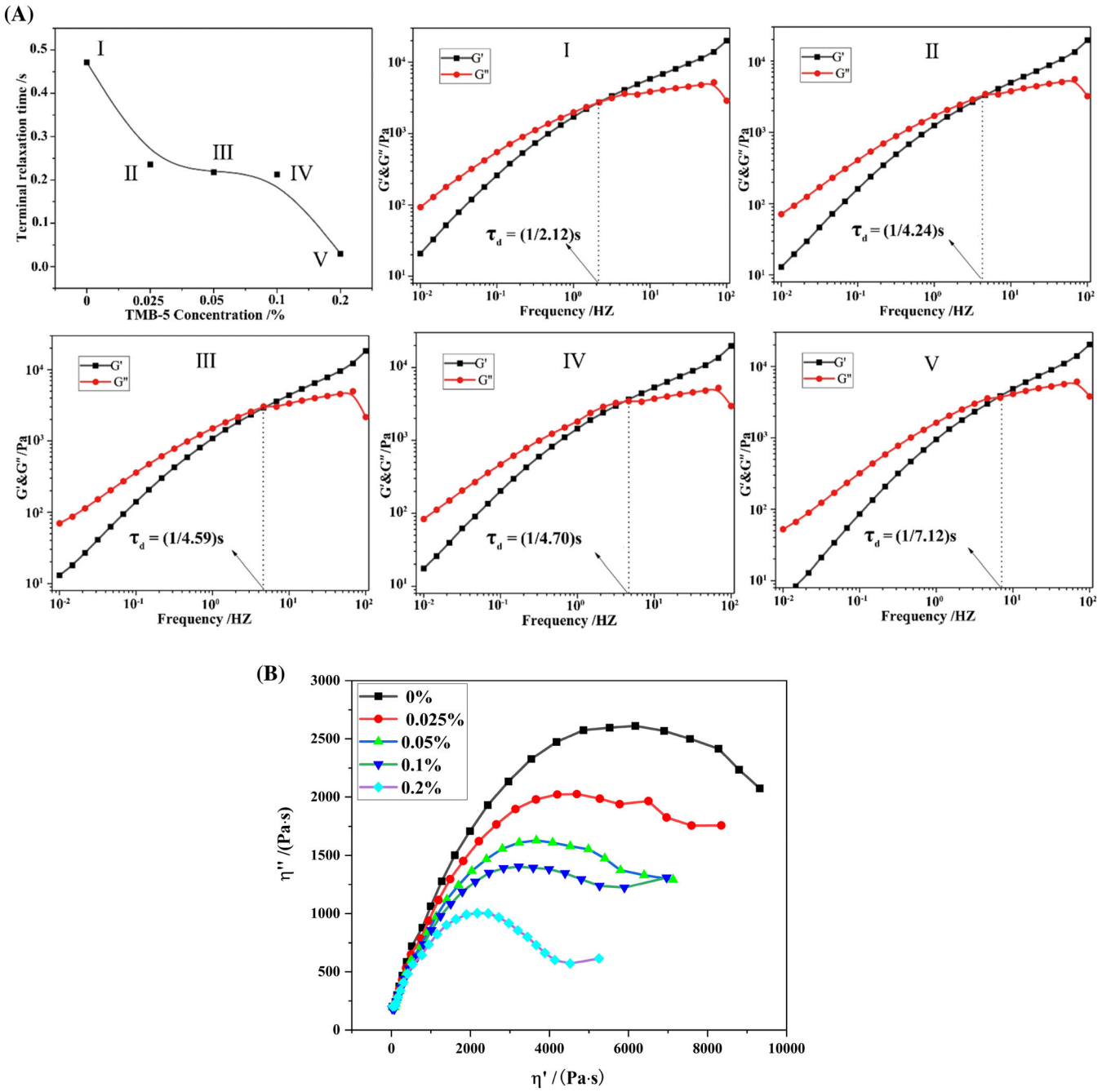

FIGURE 7 (A) The terminal relaxation time of PP at different β nucleating agent contents. (B) The Cole–Cole curves of PP at different β nucleating agent contents.

orientation. In rotating samples, induced crystallization under external force fields thickens the crystals and generates oriented crystals, resulting in a larger longer period.

3.3 | Melting behavior analysis

Figure 9 shows the DSC heating curves of static and rotating samples, with their melting peaks and crystallinity listed in Table 3. Melting curves of PP reveal that peaks above 160°C correspond to the melting of PP's α crystals, while peaks around 145°C correspond to the melting of β crystals.[30,31] From Figure 9(A), it can be observed that for static samples, pure PP pipes exhibit only one melting peak. With the increase in β-NA content, the melting point of crystals in static samples increases. After adding β-NA, two distinct melting peaks appear, indicating a significant generation of β crystals. For rotating samples, as shown in Figure 9(B–D), the

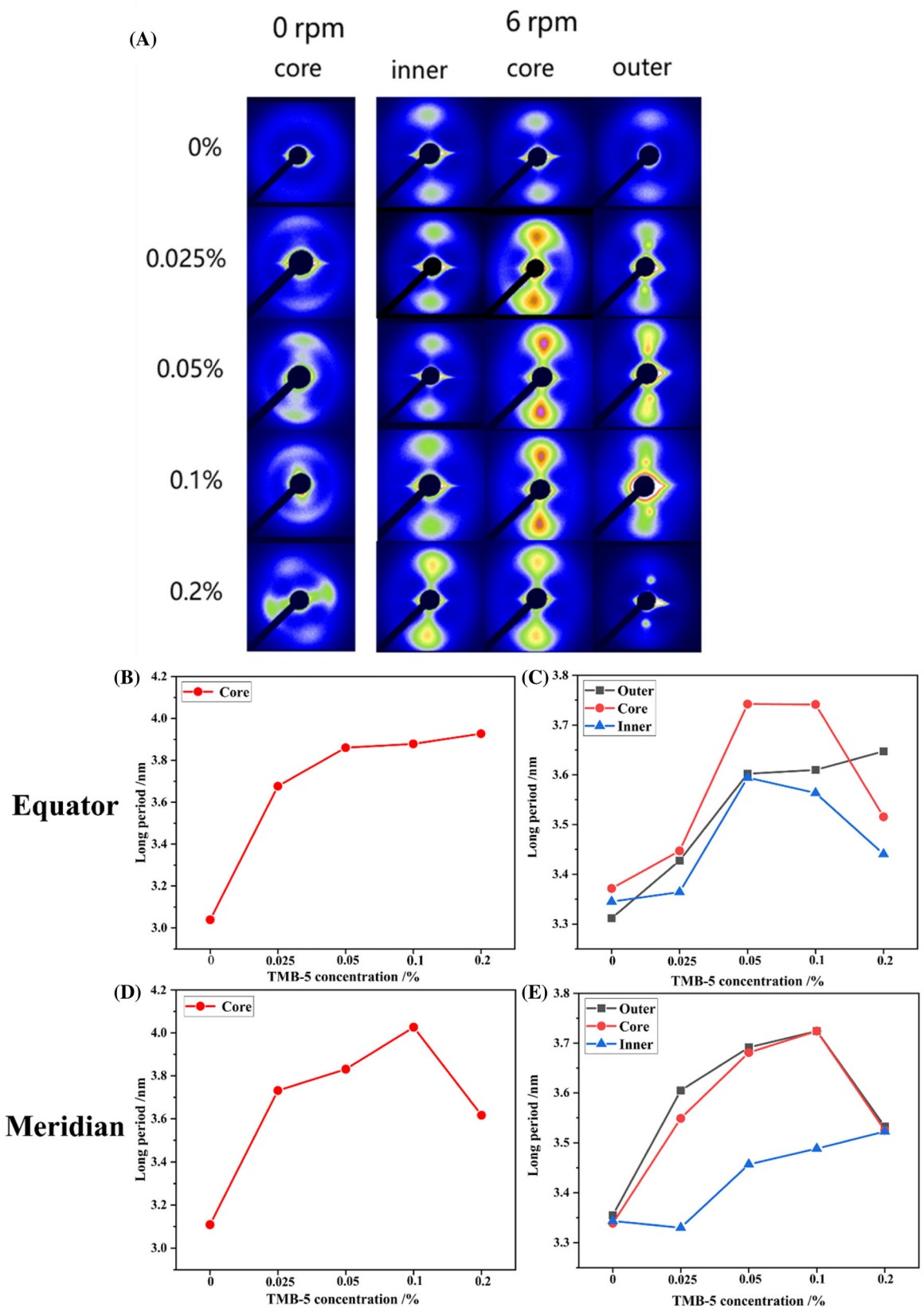

FIGURE 8 2D small-angle analysis and the long period of PP pipes in equatorial and meridian direction under different β nucleating agent contents: (A) 2D small-angle diagrams; (B) long period of static samples (0 rpm) in equatorial direction; (C) long period of static samples (0 rpm) in meridian direction; (D) long period of rotating samples (6 rpm) in equatorial direction; and (E) long period of rotating samples (6 rpm) in meridian direction.

Contents	0 wt%	0.025 wt%	0.05 wt%	0.1 wt%	0.2 wt%
D_e	2.28	1.13	1.03	1.01	0.65

TABLE 2 The *De* values of PP at different β nucleating agent contents.

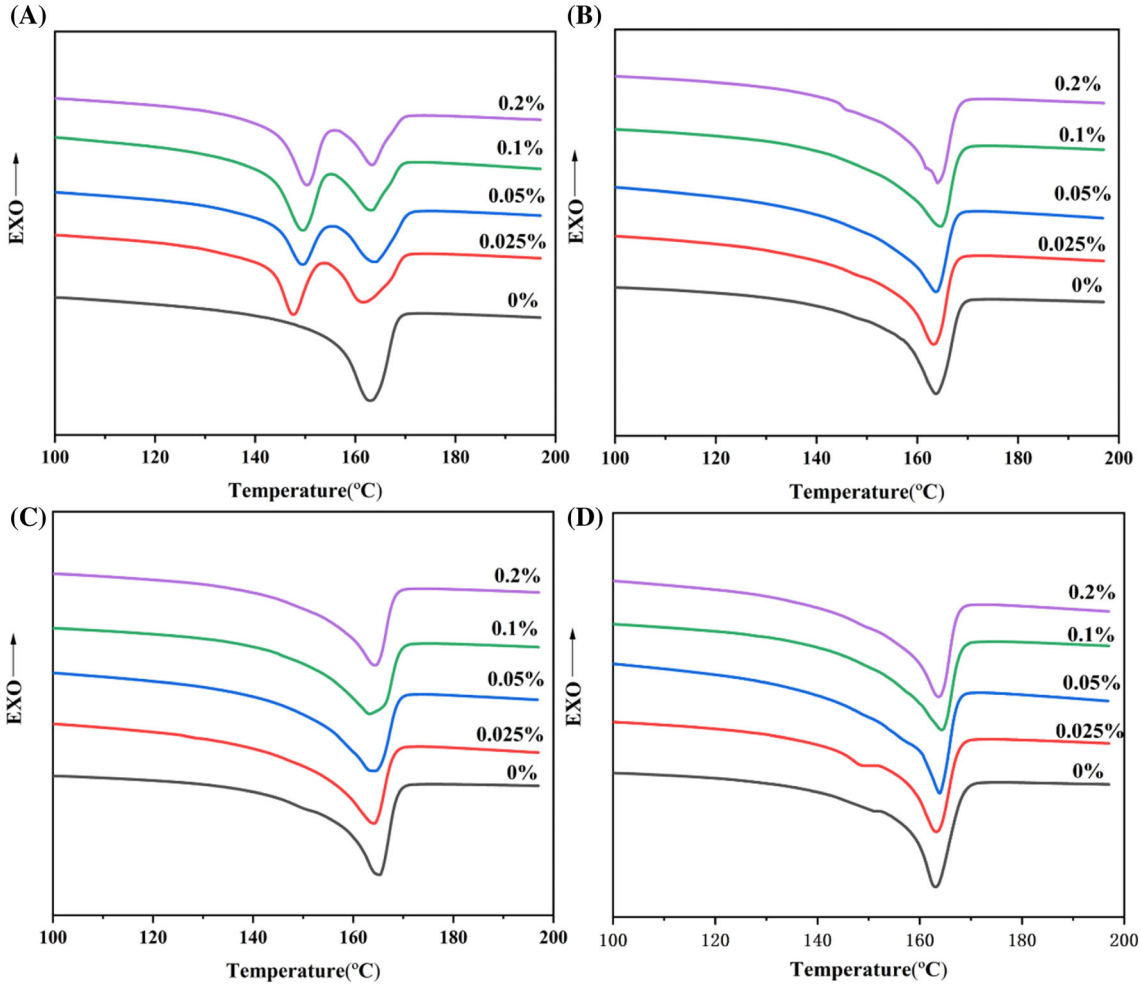

FIGURE 9 DSC heating curves of PP pipes at different β nucleating agent contents: (A) 0 rpm—middle layer; (B) 6 rpm—inner layer; (C) 6 rpm—middle layer; and (D) 6 rpm—outer layer.

melting peak of β crystals becomes less pronounced, even disappearing, consistent with the β crystal content obtained from the previous two-dimensional wide-angle analysis. For both static and rotating samples, the crystallinity initially increases and then decreases with the increase in β-NA content. Additionally, the crystallinity of rotating samples is significantly higher than that of static samples, mainly due to induced crystallization under external fields, forming a perfect crystal structure.

3.4 | Morphology analysis

Scanning electron microscopy (SEM) images were used to explore the changes in the microstructure of pipes with different β nucleating agent contents. As shown in Figure 10(A), the molecular chains are disordered in static samples (0 rpm), mainly in the form of spherulites. With a low content of β nucleating agent, the spherulites remain intact, but when the β nucleating agent content increases to 0.2 wt%, the spherulitic crystals become imperfect and exhibit a bundled morphology. This is largely related to the solubility of the β nucleating agent in PP. When its content is low, the nucleating agent is uniformly dispersed in the matrix, thereby inducing the formation of relatively perfect β spherulites. However, once the content is too high, the β nucleating agent will aggregate and precipitate in the matrix, acting as a defect that inhibits the growth of crystal structure, thus only leading to the formation of bundled structures. For

TABLE 3 The crystallinity and melting point of the middle layer of PP pipes at different β nucleating agent contents.

Contents	Rotate speed (rpm)	Melting point (°C)		Crystallinity (%)
		α crystals	β crystals	
0 wt%	0	162.73	—	47.37
	6	163.72	—	51.88
0.025 wt%	0	161.56	147.69	48.31
	6	164.07	—	49.81
0.05 wt%	0	163.95	149.43	48.45
	6	163.79	—	53.00
0.1 wt%	0	163.14	149.55	52.08
	6	163.23	—	49.28
0.2 wt%	0	163.38	150.3	47.98
	6	164.33	—	46.63

dynamic samples (6 rpm), the molecular chains in the inner layer appear to be more disordered, while they are more regular in the middle and outer layers. This is due to the inner layer reaching the solidification point earlier during the cooling process and thus experiencing a shorter shear time.

3.5 | Mechanical properties

Figure 10(B,C) shows the circumferential strength and elongation at break for conventional and rotating PP pipes across a range of β-NA contents. The tensile strength of conventional PP pipes is 33.62 MPa, with an elongation at break of 19.51%. After the application of rotational shear, both the tensile strength and elongation at break of pure PP pipes increase to 34.83 MPa and 125.78%, respectively, achieving enhanced toughness and strength. The increase in tensile strength can be attributed to orientation and shish-kebab structure, while toughening is mainly due to grain refinement.[14] For conventional samples, the presence of β crystals after adding β-NA causes the tensile strength to vary in the range of 28.80–35.35 MPa. The elongation at break of conventional samples significantly increased to 274.35% and 161.45% under the nucleating agent content of 0.025 and 0.05 wt%, respectively. Following the application of rotational shear, the tensile strength and elongation at break of rotating samples are higher than those of pure PP conventional samples at all β-NA contents. This is fundamentally different from the previous research of the same conceptual type,[11] which found that the improvement of tensile strength comes at the cost of sacrificing elongation at break. In this work, the most significant toughening effect was observed at a β-NA content of 0.025%, where the elongation at break of rotating samples reaches 243.30%. At a 0.05 wt% content, the enhancement effect is more pronounced, with the tensile strength reaching a maximum of 40.98 MPa, a 22% increase compared to the pure PP value of 33.62 MPa, and the elongation at break reaching 108.09%. Varying degrees of toughening and strengthening were also achieved at β-NA contents of 0.1% and 0.2%.

3.6 | Creep behavior analysis

To better explain the influence of the change of microstructure on the long-term performance of PP pipes, we selected samples with relatively high orientation and crystallinity for testing, as well as static samples for comparison. Figure 11(A,B) represent the variation curves of strain and compliance with time for all specimens. It can be observed that after applying a certain load, all specimens undergo instantaneous deformation, primary creep, and secondary creep. Regardless of the presence of β nucleating agents, the strain and compliance of rotating pipes (red and green lines in the figures) are much smaller than those of static pipes (black and blue lines in the figures), indicating that rotating pipes have much stronger resistance to deformation than static pipes. This is because during the creep of polymers, once internal lamellae bear external forces and store energy, bending to a certain critical value, large lamellar units will rupture into smaller lamellar units, and there will also be dislocations, transfers, or divisions between lamellar units. Therefore, a large amount of orientation and fibrillar structures formed by rotating pipes enhances the interconnection between molecular chains or lamellae, effectively preventing processes such as untying, slipping, and debonding between molecular chains, thereby improving deformation resistance.[32] On the other hand,

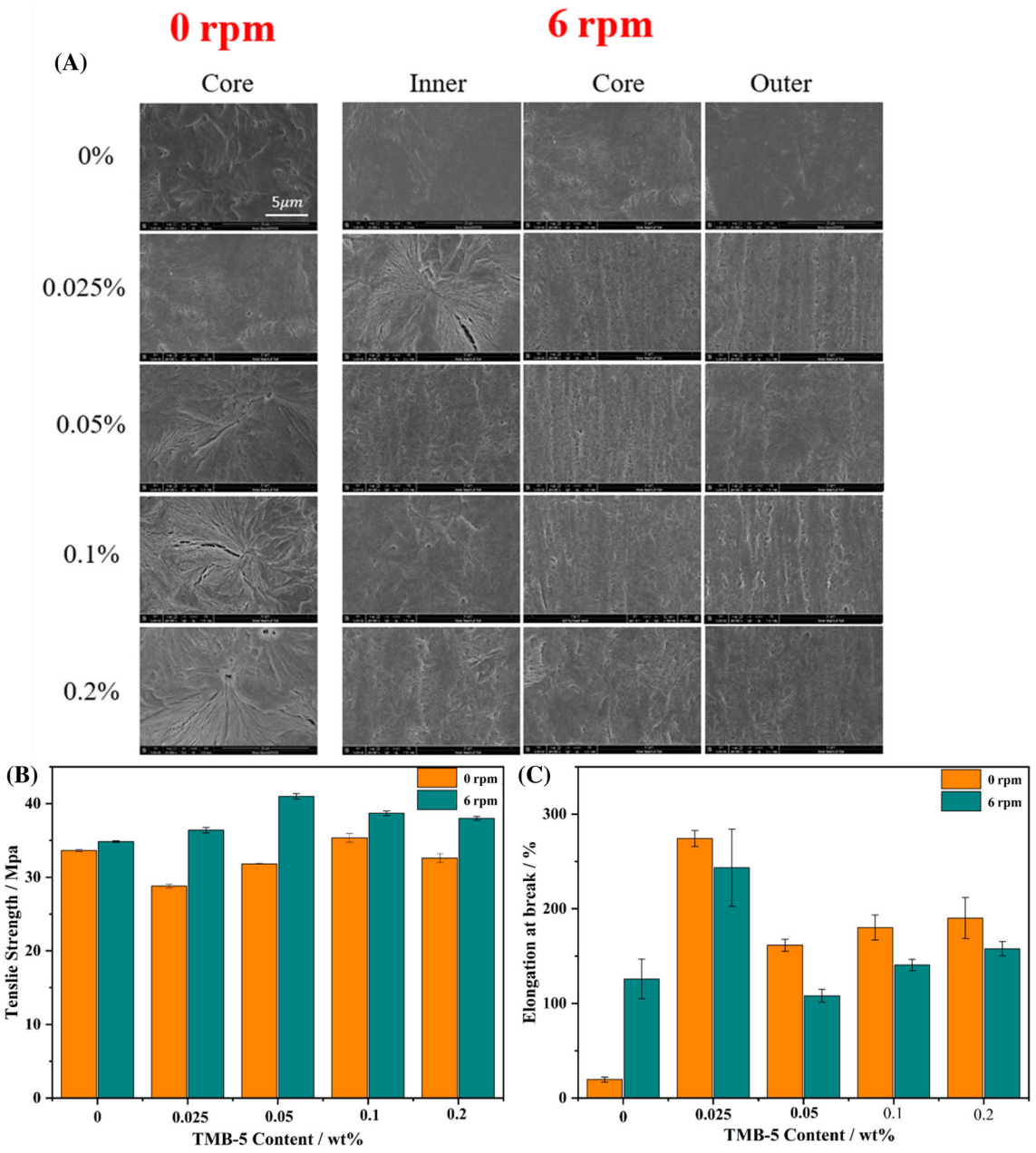

FIGURE 10 The morphology images and mechanical properties of PP pipes with varying contents of β nucleating agents: (A) SEM images. (B) Tensile strength. (C) Elongation at break.

previous studies have reported that compliance decreases with increasing crystallinity.[33] The crystallinity of rotating pipes is significantly higher than that of static pipes, making the tie molecules in rotating pipes more robust and less susceptible to untangling and slipping, naturally resulting in better resistance to external force-induced slippage.

Among static specimens, the strain and compliance of pure PP (black lines in the figures) are lower than that of PP pipes with added β-NA (blue lines in the figures), indicating better creep performance. The internal arrangement of the β crystals is looser than that of the α crystals,[27] and molecular chains are more prone to slippage. Therefore, pipes containing more β crystals have relatively low creep resistance. In contrast, in the two rotating specimens (pure PP for red lines and PP added β-NA for green lines), this trend is reversed, and the creep performance of PP pipes with added nucleating agents is better than that of pure PP pipes due to the smaller strain and compliance. Apparently, the content of β crystals has little influence on this different trend compared with static specimens, as the results of DSC show that the β crystal contents of the rotating samples are very low. However, the results of WAXD show that

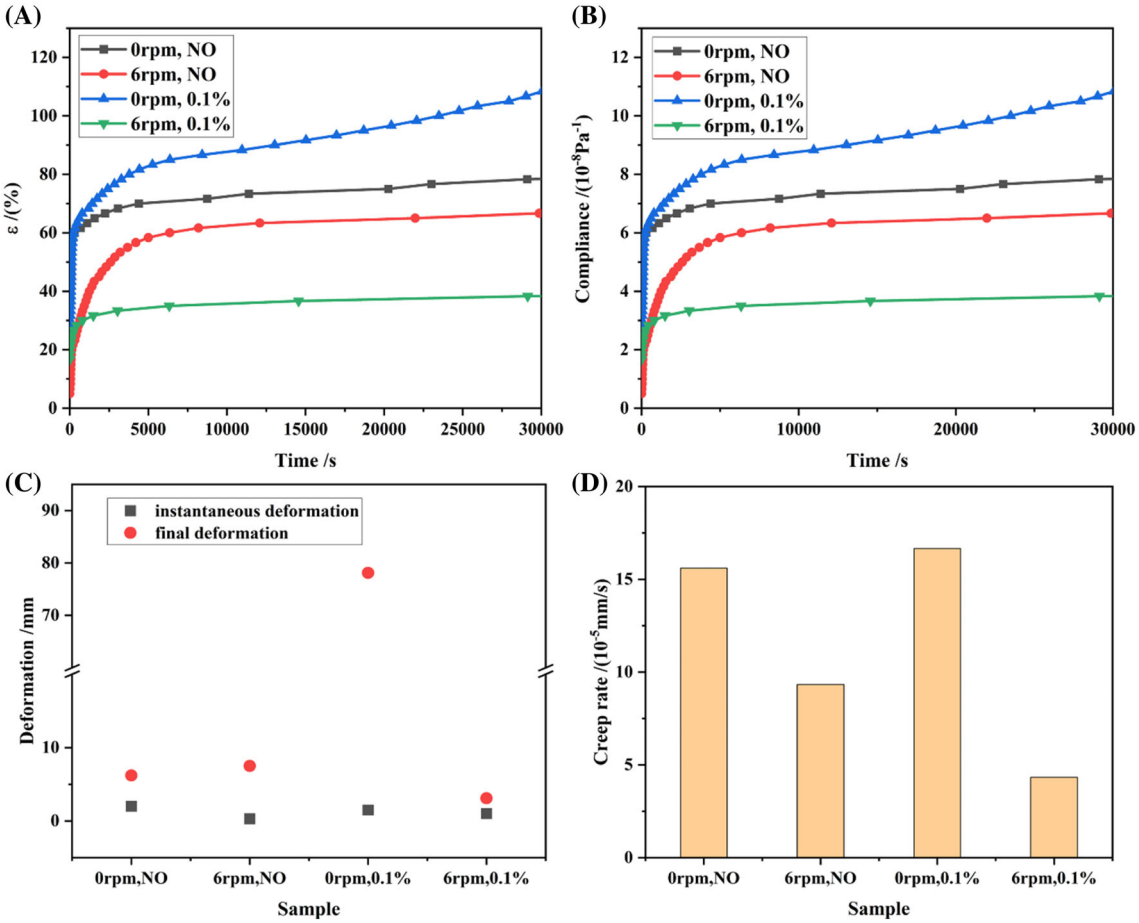

FIGURE 11 Creep behavior results in schematic diagram: (A) Creep curves of different specimens. (B) Compliance curves of different specimens. (C) Initial displacement and final displacement. (D) Creep rate.

rotating PP pipes with added β nucleating agents have a higher degree of orientation because of increased shear rate and decreased relaxation time, thus possessing better resistance to external force-induced slippage.

Instantaneous and final deformations of each pipe specimen were presented in Figure 11(C). The initial displacement of the pure sample (0 rpm) and the sample with nucleating agent (0 rpm, 0.1%) was 2.3 and 2.4 mm, respectively. The rotating pipes exhibit lower initial displacements at 0.8 mm (6 rpm, NO) and 1.8 mm (6 rpm, 1%). Among all specimens, static pipes with added β nucleating agents (0 rpm, 0.1%) exhibit the largest final deformation, 76.9 mm, much higher than the other three specimens, mainly due to having the highest β crystal content, which is further proved by WAXD patterns having highest brightness of β (300) planes. Figure 11(D) compares the creep rates of each pipe specimen. Static pipes with added β nucleating agents have the highest creep rate at 17.84×10^{-5} mm/s, while rotating pipes with added β nucleating agents have the lowest creep rate at 3.23×10^{-5} mm/s. The creep rate of rotating pipes is lower than that of static specimens, indicating that the creep resistance of rotating pipes has been significantly improved.

3.7 | Analysis of slow crack growth

Figure 12(A) shows the morphology images of slow crack growth in pure PP pipes under static conditions. The annotations on the image include time in the top left corner and the crack width at the center. When the pipe is inserted into the brass cone, the pre-cut 1 mm notch is only widening slightly to 1.099 mm, due to the external force. This only causes a change in crack angle rather than forward propagation, because of the low stress level and the time required for tie molecules to be pulled out from the crystalline region. After 21 h, the failure occurred within the silver streaks, and the crack began to propagate forward, forming a crack of 0.455 mm at the front end. This time can be taken as the crack growth initiation time, which can be obtained by linear regression analysis of crack width versus time. Subsequent images were taken every 3 h, and the crack width showed a

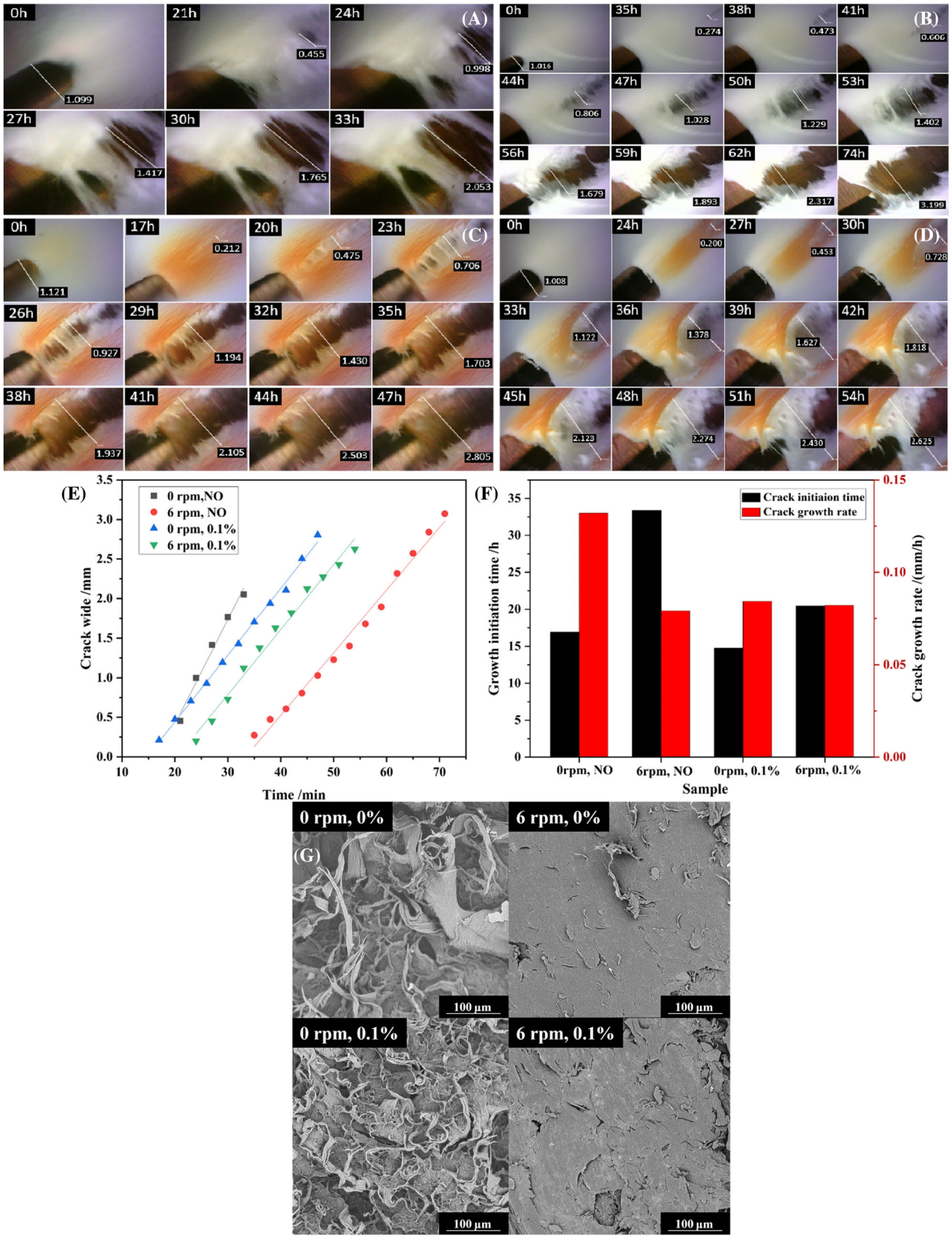

FIGURE 12 Analysis of slow crack growth: (A) The slow crack growth process of pure PP static pipe (0 rpm, NO). (B) The slow crack growth process of pure PP rotating pipe (6 rpm, NO). (C) The slow crack growth process of pure PP static pipe (6 rpm, 0.1%). (D) The slow crack growth process of β nucleating agent-added rotating PP pipe (6 rpm, 0.1%). (E) Crack width vs. time. (F) Crack initiation time and crack growth rate. (G) The cross-sectional morphology of each specimen.

linear increase. It can be seen that filamentation is obvious during the crack growth process from 24 to 33 h. In the later stages, the filaments were not pulled apart, indicating that the molecular chains of the static specimen were initially in an amorphous state and formed highly oriented microfibers under external stress, which, to some extent, indicates a ductile fracture mode.

Slow crack growth in pure PP pipes under rotational shear conditions was presented in Figure 12(B). Compared to static PP pipes, the initiation stage of the crack was significantly prolonged, with the crack becoming evident around 35 h. At 74 h, the specimen had not completely fractured, indicating the improved resistance to slow crack growth. It was observed that the crack growth did not take place from the pre-cut notch but instead at a distance from it, and then the crack gradually extended to the notch. As the crack develops in the later stages, the material adjacent to the crack undergoes direct rupture without much filamentation, exhibiting characteristics of brittle fracture. This is because the molecular chains of the dynamic specimen were already aligned in a highly oriented state before stretching, resulting in less plastic deformation.

When the pre-cut notch was applied to the PP static pipes with added β NA, the width of the notch immediately expanded to 1.121 mm, as shown in Figure 12(C). The initiation time of the crack was the shortest, at 17 h, indicating that the molecular chains in this specimen were more prone to slip. After the molecular chains disentangle from the crystalline region, crystal plane slip and bending fracture are more likely to occur. Many fine filaments were observed, indicating a ductile fracture mode. Figure 12(D) displays the morphology images of slow crack growth in rotating PP pipes with added β nucleating agents. When the pre-cut notch was applied to the specimen, the width of the notch remained at a minimum value among all specimens, at 1.008 mm. The initiation time of the crack was approximately 24 h, the longest among all the specimens, indicating that the long-term mechanical performance of rotating field pipes was enhanced.

It can be seen in Figure 12(E), the crack width of all specimens exhibits linear growth after a certain period. Dynamic specimens present a delayed onset, indicating better resistance to slow crack growth. By linearly fitting crack width against time, the intersection of the trend line with the x-axis is defined as the crack initiation time. The slope of the trend line is defined as the crack growth rate, as shown in Figure 12(F). Compared to the two static specimens, the crack initiation time of the two dynamic specimens is longer, and the crack growth rate is lower, indicating better resistance to slow crack growth. The oriented structure of dynamic specimens is an important factor in improving resistance to slow crack growth. Slow crack growth mainly occurs when many tie molecules detach from a single crystal, forming macroscopically visible cracks. Molecular chains are oriented along the circumferential direction of the pipe, significantly increasing the number of tie molecules. Under external stress, a greater number of tie molecules share the stress, making it more difficult to extract tie molecules from the crystals and thereby enhancing resistance to slow crack growth.[34] In dynamic specimens, the crack initiation time of pure PP pipes is longer than that of PP pipes with added β nucleating agents, while the difference in crack growth rate is minimal. This is contrary to the resistance to creep, mainly because their mechanisms are different. A small amount of β crystals can still be generated in PP pipes with added β nucleating agents after rotation, and the relatively loose structure of β crystals weakens the binding force of crystals to tie molecules, making tie molecules easier to extract. Therefore, the resistance to slow crack growth is relatively weak.

Figure 12(G) presents the cross-sectional morphology after slow crack growth for each specimen. It can be observed that the static specimens (0 rpm) exhibit a rough surface composed of elongated features with many voids, indicating a complete plastic deformation in a ductile fracture mode. In contrast, the dynamic specimens (6 rpm) show a relatively smooth surface with layered fracture, indicating a brittle fracture mode. The significant difference in fracture mode between static and dynamic specimens of the same material resulted from the molecular chain orientation.

4 | CONCLUSIONS

The morphology and mechanical properties of PP pipes with added β nucleating agents were studied using an in-house designed RSS operated at different mandrel speeds. The results showed that due to changes in crystal phase and orientation structures, the mechanical properties of PP pipes with different β-NA contents varied. Overall, the most significant toughening effect was observed at a 0.025% nucleating agent content, where the tensile strength of the rotating specimens increased while the elongation at break reached 243.30%. Additionally, the rotating pipes with added β nucleating agents exhibited the best resistance to creep. Although their resistance to slow crack propagation was not as good as that of rotating pipes without β nucleating agents, they were still stronger than conventional pipes. Detailed SAXS and SEM studies revealed the development process of spherulites and the trend of long-period development throughout the entire rotating shear

process. X-ray diffraction, DSC, and SEM analyses showed changes in β crystal content, orientation, crystallinity, and grain refinement. At a 0.05 wt% nucleating agent content, the reinforcement effect was optimal, with the maximum tensile strength reaching 40.98 MPa, a 22% increase compared to pure PP (33.62 MPa), and the elongation at break also reached 108.09%.

ACKNOWLEDGMENTS

The authors gratefully thank the financial support from the National Natural Science Foundation of China (Grant Nos. 52373045, 12375332, 52033005, and 21627804). We are also indebted to the Shanghai Synchrotron Radiation Facility (SSRF) in Shanghai, China, for WAXD and SAXS experiments.

DATA AVAILABILITY STATEMENT

All data generated or analyzed during this study are available on reasonable request.

ORCID

Aerman Abudurezhake https://orcid.org/0009-0004-1376-2159

REFERENCES

1. Yesil Y, Bhat GS. Structure and mechanical properties of polyethylene melt blown nonwovens. *Int J Cloth Sci Technol*. 2016;28:780-793.
2. Worth RA. Effect of mandrel rotation on power-consumption in polypropylene extrusion. *Polym Eng Sci*. 1979;19:198-202.
3. Awaya H. Morphology of different types of isotactic polypropylene SPHERULITES crystallized from melt. *Polymer*. 1988;29:591-596.
4. Zhang J, Shen K, Na S, Fu Q. Vibration-induced change of crystal structure in isotactic polypropylene and its improved mechanical properties. *J Polym Sci Pt B-Polym Phys*. 2004;42:2385-2390.
5. Varga J. Beta-modification of polypropylene and its 2-component systems. *J Thermal Anal*. 1989;35:1891-1912.
6. Liu H, Huo H. Competitive growth of α- and β-crystals in isotactic polypropylene with versatile nucleating agents under shear flow. *Colloid Polym Sci*. 2013;291:1913-1925.
7. Zhou SY, Niu B, Xie XL, et al. Interfacial shish-kebabs lengthened by coupling effect of in situ flexible nanofibrils and intense shear flow: achieving hierarchy to conquer the conflicts between strength and toughness of polylactide. *ACS Appl Mater Interfaces*. 2017;9:10148-10159.
8. Gu XB, Zhou M, Wang YX, Zhang J. Influence of annealing on the morphology and mechanical properties of iPP/HDPE blend with tailored oriented crystalline structures. *J Polym Res*. 2019;26:11.
9. Nie M, Wang Q. Control of rotation extrusion over shish-kebab crystal alignment in polyethylene pipe and its effect on the pipe's crack resistance. *J Appl Polym Sci*. 2013;128:3149-3155.
10. Men YF, Rieger J, Enderle HF, Lilge D. The mobility of the amorphous phase in polyethylene as a determining factor for slow crack growth. *Eur Phys J E*. 2004;15:421-425.
11. Luo XH, Pan YX, Li YC, et al. Effect of oscillatory shear field on the morphology and mechanical properties of β-nucleated isotactic polypropylene. *Polym Eng Sci*. 2017;57:838-845.
12. Han R, Nie M, Bai SB, Wang Q. Control over crystalline form in polypropylene pipe via mandrel rotation extrusion. *Polym Bull*. 2013;70:2083-2096.
13. Guo Y, Wang Q, Bai SB. The effect of rotational extrusion on the structure and properties of HDPE pipes. *Polym-Plast Technol Eng*. 2010;49:908-915.
14. Wu JJ, Xie ZX, Yang H, et al. Effect of mandrel rotation speed on morphology and mechanical properties of polypropylene pipes produced by rotational shear. *J Polym Res*. 2021;28:13.
15. Yang H, Luo XH, Shen KZ, et al. The role of mandrel rotation speed on morphology and mechanical properties of polyethylene pipes produced by rotational shear. *Polymer*. 2019;184:11.
16. Dong M, Guo ZX, Su ZQ, Yu JA. The effects of crystallization condition on the microstructure and thermal stability of Istactic polypropylene nucleated by β-form nucleating agent. *J Appl Polym Sci*. 2011;119:1374-1382.
17. Turnerjones A, Cobbold AJ. Beta crystalline form of isotactic polypropylene. *J Polym Sci, Part B: Polym Phys*. 1968;6:539.
18. Mi DS, Liu H, Zhang L, Wang T, Zhang XW, Zhang J. The changes of microstructure and physical properties of isotactic polypropylene/β nucleation agent/polyolefin elastomer induced by annealing following processing. *J Macromol Sci Part B-Phys*. 2015;54:1376-1390.
19. Coppola S, Grizzuti N, Maffettone PL. Microrheological modeling of flow-induced crystallization. *Macromolecules*. 2001;34:5030-5036.
20. Heeley EL, Fernyhough CM, Graham RS, et al. Shear-induced crystallization in blends of model linear and long-chain branched hydrogenated polybutadienes. *Macromolecules*. 2006;39:5058-5071.
21. Rathee V, Krishnaswamy R, Pal A, et al. Reversible shear-induced crystallization above equilibrium freezing temperature in a lyotropic surfactant system. *Proc Natl Acad Sci U S A*. 2013;110:14849-14854.
22. Chen YH, Mao YM, Li ZM, Hsiao BS. Competitive growth of α- and β-crystals in β-nucleated isotactic polypropylene under shear flow. *Macromolecules*. 2010;43:6760-6771.
23. Huo H, Jiang SC, An LJ, Feng JC. Influence of shear on crystallization behavior of the β phase in isotactic polypropylene with β-nucleating agent. *Macromolecules*. 2004;37:2478-2483.
24. Graebling D, Muller R, Palierne JF. Linear viscoelastic behavior of some incompatible polymer blends in the melt - interpretation of data with a model of emulsion of viscoelastic liquids. *Macromolecules*. 1993;26:320-329.
25. Varga J, Menyhárd A. Effect of solubility and nucleating duality ofN,N'-Dicyclohexyl-2,6-naphthalenedicarboxamide on the supermolecular structure of isotactic polypropylene. *Macromolecules*. 2007;40:2422-2431.
26. Dong M, Gu ZX, Yu J, Su ZQ. Crystallization behavior and morphological development of isotactic polypropylene with an aryl amide derivative as β-form nucleating agent. *J Polym Sci Pt B-Polym Phys*. 2008;46:1725-1733.
27. Meille SV, Ferro DR, Bruckner S, Lovinger AJ, Padden FJ. Structure of BETA-isotactic polypropylene - a long-standing structural puzzle. *Macromolecules*. 1994;27:2615-2622.
28. Natta G, Corradini P. Structure and properties of isotactic polypropylene. *Nuovo Cim*. 1960;15:40-51.

29. Larin B, Avila-Orta CA, Somani RH, Hsiao BS, Marom G. Combined effect of shear and fibrous fillers on orientation-induced crystallization in discontinuous aramid fiber/isotactic polypropylene composites. *Polymer*. 2008;49:295-302.
30. Lotz B. α and β phases of isotactic polypropylene: a case of growth kinetics 'phase reentrency' in polymer crystallization. *Polymer*. 1998;39:4561-4567.
31. Varga J, Ehrenstein GW. Formation of beta-modification of isotactic polypropylene in its late stage of crystallization. *Polymer*. 1996;37:5959-5963.
32. Young RJ. Dislocation model for yield in polyethylene. *Philos Mag*. 1974;30:85-94.
33. Nitta K, Maeda H. Creep behavior of high density polyethylene under a constant true stress. *Polym Test*. 2010;29:60-65.
34. Cao JG, Gao XQ, Shen KZ. Influence of shish-kebab structure on the shortdated mechanical property of self-enhancement HDPE and performance of resist slow crack growth. *Eur Polym J*. 2012;44:200-206.

SUPPORTING INFORMATION

Additional supporting information can be found online in the Supporting Information section at the end of this article.

How to cite this article: Abudurezhake A, Yang M, Gong J, et al. Effect of β nucleating agent and rotational shear on morphology and mechanical properties of polypropylene pipes. *Polym Eng Sci*. 2024;1-19. doi:10.1002/pen.26982